Fast and Accurate Retinal Identification System: Using Retinal Blood Vasculature Landmarks

***Abstract*—While technological advances in automation have made life easier, it has introduced major security threats. To deal with the increasing rate of e-commerce fraudulent activities and identity theft, it is crucial to elevate automated identification systems. We present a high-performance fast and accurate approach for retinal identification. The proposed approach achieved high recognition accuracy by using such features that have maximum discriminant power among the classes and completely eliminated overlapping. Segmentation accuracy is improved by using different and separate segmentations for thick and thin blood vessels. In contrast to other techniques which focused only on accuracy, time efficiency is also targeted alongside accuracy in this work. Our method is made fast and computationally time efficient via principal component analysis. The proposed technique is validated on DRIVE, STARE, VARIA, RIDB, HRF, Messidor, DIARETDB0, and a multi-sample per subject database created by authors using the images provided by Dr. Chen (Shanghai Jiao Tong University Affiliated Sixth People's Hospital). Experimental results demonstrated that the proposed approach outperforms other existing techniques. Segmentation achieves an overall accuracy of 99.65% with the recognition rate of 99.40% on all these databases.**

***Index Terms*—Biometrics, PCA, retinal identification.**

I. Introduction

THE expansion of automation technologies and increased risk of identity theft have led emphasis on the need of automated identification systems. Biometric authentication is used for people identification based on their physical and behavioral traits [1]. Biometric traits can be used for identification of face, fingerprint, ear, retina, iris, palm print, speech, signature, keystroke dynamics, gesture, and gait [2], [3], [4], [5]. Biometrics has observed a significant evolution from facial to speech recognition [6], [7]. Although commonly used biometric identifiers provide a high level of security, yet they are susceptible to forgery and variations. So, the permanence required for biometrics can be breached. To overcome these challenges, the alternate solution is to use retina as a biometric variant. The retina is an internal organ that lies at the back end of the eye which makes it resistant to forgery. Its morphological structure contains unique features as shown in Fig. 1. These features provide the basis for the distinction between different subjects [8], [9].

Previous researches on retinal identification mainly focused on: a) Reliable vasculature network extraction or feature points extraction and not on time efficiency [10], [11], [12], [13], [14]; b) Used end points, bifurcations, crossing over, a combination of end points and bifurcation, a combination of bifurcations and crossing over, optic disc location as features [4], [13], [15], [16], [17]. All these features provide distinction, but with an overlap between classes (authenticated and intruder). This overlapping reduces recognition accuracy; c) Used single segmentation technique for both thick and thin blood vessels [18], [19], [20], [21]. However, with a single segmentation technique, thin vessels get discarded. When thin vessels get discarded, the overall segmentation accuracy is reduced.

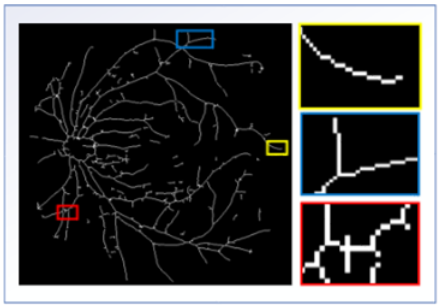

Fig. 1: Human Retinal Vasculature Network. End point, bifurcation, and crossing point are used as feature by the proposed system. Each of these feature points have been highlighted (Yellow = end point, Blue = bifurcation, Red = crossing over).

Motivated by these issues, this paper aims to: a) Accelerate the matching process to make identification fast, computationally cost effective and time efficient. This acceleration and efficiency will make it more suitable for real-time applications. b) Selection of such features that provide maximum discriminant power to improve recognition accuracy. c) Use an efficient segmentation technique to improve the segmentation accuracy. Our work makes the following three main contributions:

- **Efficient and fast matching process** Principal component analysis (PCA) [22] based accelerated retinal identification system is proposed. The extracted features are projected into a subspace achieved by PCA. This dimension reduction significantly reduces computation time and accelerates the matching process.
- **Enhanced discriminant power features** A combination of end points, bifurcation, and crossing over is used. Experimental results showed that the in contrast to other techniques the proposed features combination completely eliminated overlap between classes and has maximum discriminant power. It results in improved identification accuracy.
- **Improved segmentation accuracy** Separate segmentations are used for thick/thin blood vessels. The use of hybrid segmentation is more effective to retain complete retinal vasculature. It prevents thin vessels from being discarded. That helps to improve segmentation accuracy.

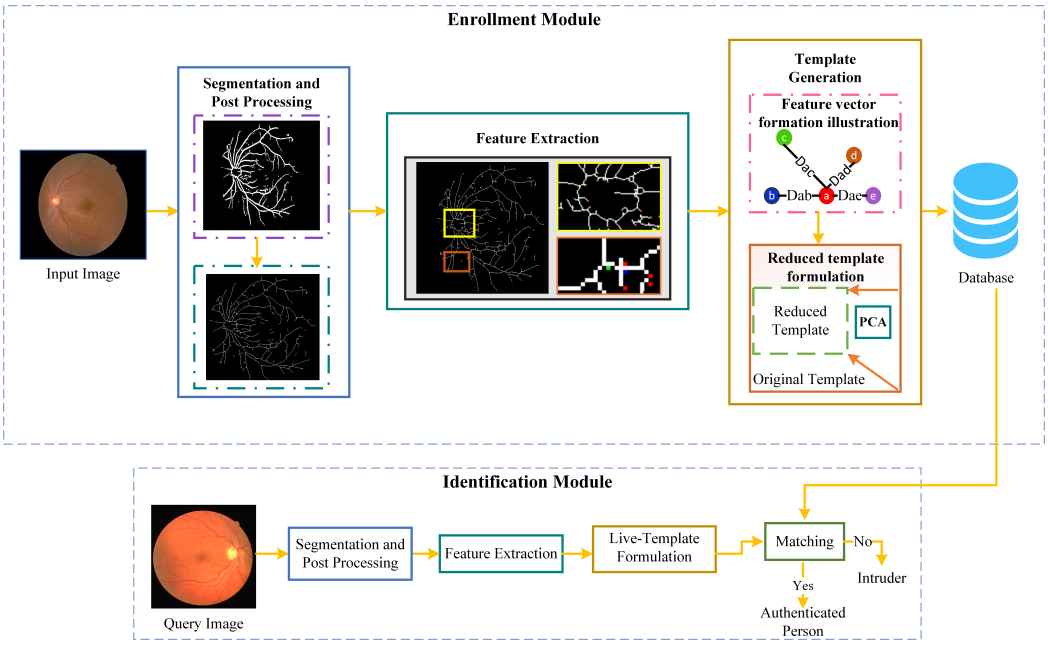

Fig. 2: Overview of the proposed approach. Enrollment and identification a re t wo m ain m odules. E nrollment module:- Segmentation and Post-Processing: The result of the final s egmentation a nd s keletonization i s s hown. F eature Extraction: Features are extracted and highlighted using color slicing. Zoomed images depict the result of color slicing. Template Generation: Feature vector formation illustration: "a" is the candidate feature point. Distance and angle between "a" and its four nearest feature points "b", "c", "d", and "e" are found to formulate feature vector. Reduced template formulation: PCA is applied for dimensionality reduction. The reduced template is then stored in the database. Identification Module:- Live-Template Formulation: Query image template (live-template) is generated. Matching: L2-norm is used to find the distance between live-template and templates stored in the database. Depending on the distance, total similarity measure (TSM) is calculated. Query image is given a status either authenticated or intruder based on TSM.

II. Related Work

EyeDentify company provided the first commercially available retinal identification system that uses a retina scanner called EyeDentification [23]. It maps vascular pattern on the retinal portion of the eyeball. Sadikoglu and Uzelaltinbulat [24] used the feature vector of the segmented image with a neural network. The neural network is trained by back-propagation. Fatima et al. [15] used a recursive supervised multilayered thresholding for accurate segmentation. Vascular ending and bifurcation are used as features. Mahalanobis distance is used as a similarity measure for identification. In [17], feature extraction is performed by using optic disc location as a reference point. Blood vessels that are around optic disc are used for feature generation. Köse et al. [25] proposed a retinal identification that employed a similarity measure and is capable of tolerating the transformations. In [11], Fourier transform coefficient and angular partitioning are used for feature detection. Euclidean distance is used in the matching process. Monisha and Seldevchristopher [12] used the crossing number technique to find features and voting for finding similarity. Sasidharan [14] used skeletonization for feature extraction. Similarity transformation is used for similarity check between reference and candidate image.

Akram et al. [13] formulated feature vector by calculating distance and angle between feature points. Bifurcation is the chosen feature point. The accuracy was further improved by using both bifurcation and end points as features in [4]. Gabor filter is used for extraction of feature points. The resulting feature vectors are stored in the database. The reference image and candidate images are matched using a SVM classifier [26]. In [16], branch points and crossing points are extracted from only those vessels that have a certain width. Geometric hashing is used to make features invariant. Crossing points and branch points are used to map the hash table for every image. Jiu et al. [27] used Gabor wavelet transform for enhancement of vessels. The feature vector is formed by calculating distance and angle between four nearest neighbors of a feature point. Euclidean distance is used to test authentication.

III. Approach Overview

Fig. 2 gives an overview of the proposed system. It comprises of two main modules: Enrollment and Identification. Enrollment module comprises of pre-processing, segmentation, post-processing, feature extraction, template generation and registration to database submodules. Identification module comprises of live-template formulation and matching submodules. Pre-processing is specifically used to remove artifacts. Feature extraction is used for features extraction. After that, angle and distance between a feature point and its four nearest feature points are calculated to formulate the template. Template dimensionality is then reduced by PCA. This step is crucial as it hastens the matching process

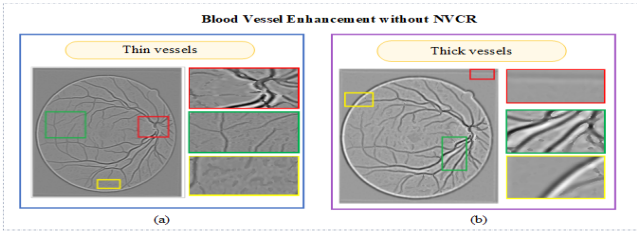

Fig. 3: (a) Thin vasculature obtained without using NVCR: Zoomed images show artifacts. Red = optic disc boundary is apparent, Green = blood vessels are not enhanced properly and somewhat suppressed, Yellow = noise is also present and has a similar texture to that of vessels. (b) Thick vasculature obtained without using NVCR. Red = non-uniform background, Green = illumination is present around blood vessels, Yellow = retinal boundary is also highlighted and there is no distinction between foreground and background.

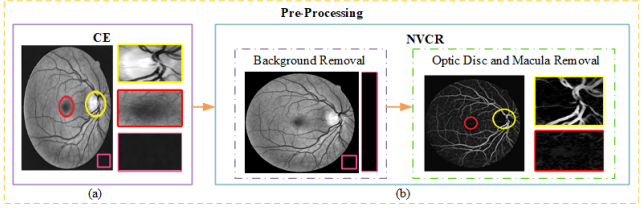

Fig. 4: Pre-processing. (a) CE module: Enhanced image obtained by applying CLAHE on $I_{gchannel}$. Zoomed images show NVC. Yellow = optic disc, Red = macula, Pink = background with noise. (b) NVCR module: Background removal: Removes the artifacts and noise in the background by masking enhanced image with mask. Zoomed image shows a complete black background with no noise. Optic Disc and Macula Removal: Modified Top-Hat Transform is applied for removing optic disc and macula.

and gives the proposed technique a lead over other existing techniques. After that in registration to database submodule, dimensionality reduced templates are stored in the database. In the identification module, the query image is given to system and its live-template is generated. L2-norm is used to calculate the distance between the feature vector of live-template and the feature vector of all the templates stored in the database. Based on the distance TSM is calculated. The result of this matching is a list of TSM between live-template and templates stored in the database. The subject with which live-template has maximum TSM is considered a match. If TSM is less than a pre-defined threshold then the query image corresponds to an intruder.

IV. Enrollment Module

A. Pre-Processing

The presence of noise in retinal images can render them inappropriate for identification phase [28], [29]. Retinal images contain non-uniform illuminations, blurry areas, and noisy background. Noise seems to be present in regions with poor illumination and is more prominent closer to retinal edges [30], [31]. Eye movements cause motion artifacts that induce blurring in images. Noise can also be induced by image acquisition modality i.e. Fundus camera [32]. Thus, pre-processing is used for artifacts exclusion and to make images appropriate for reliable feature extraction. Pre-processing is of vital significance as the overall strength of retinal identification depends on the final segmented image. To deal with variations of different data sets, standardization is done to make the proposed technique universal for all of the data sets. Through experiments, the resolution of 256×256 is found to be optimal for performance. Thus, all images are resized to the resolution of 256×256.

1) Contrast Enhancement (CE): Green channel contains fine details and valuable information. So, to obtain maximum contrast between the blood vessels and background green channel is extracted. To make intensity uniform and to remove non-uniform illuminations from the images, Contrast Limited Adaptive Histogram Equalization (CLAHE) [33] is applied. CLAHE divides the image into non-overlapping regions termed as tiles. Contrary to conventional contrast enhancement methods, it prevents over-amplification of noise by using a predefined value termed as clip limit [33]. There is no need for adaptive selection of CLAHE parameters because image size has been fixed to the resolution of 256×256. To select an appropriate clip limit for CLAHE, we varied clip limit from 0.01-0.05. With a clip limit of 0.01, the image quality was improved, the noise level was low and blood vessels were perceivable as well. To select tile size, we varied it from $[8 \times 8]$ to $[64 \times 64]$ and compared corresponding processing time. With different images, a window size of $[8 \times 8]$ had the least processing time. So for experiments, a clip limit of 0.01 and window size of $[8 \times 8]$ is applied to the extracted green channel $(I_{gchannel})$ for optimum performance.

2) Non-Vascular Components Removal (NVCR): Segmentation process is accelerated by removing non-vascular components (NVC). NVC constitute of background, optic disc, macula, and other abnormalities. If NVC are not removed, the processing time will be more, blood vessels will not be enhanced appropriately, the noise will be more apparent, there will be non-uniform background, the computational cost of successive methods will be more and NVC will appear as false positive during segmentation stage. These artifacts are clearly visible in Fig. 3. All these factors result in declined performance. So, NVCR has a crucial role in handling the general performance of the proposed system.

The region of interest (ROI) in retinal images corresponds to the semi-circular region over a dark background [30]. The background is not actually black, but it contains noise [34]. So, it is necessary to mask the pixels that do not constitute ROI. Mask image is created by a two-stage process: coarse level and fine level. At the coarse level, Otsu threshold algorithm [35] is applied to $I_{gchannel}$. However, some pixels are misclassified at this stage. At the fine level, these pixels are classified correctly by morphological opening and closing operation with a disc-shaped structuring element having radius 2. After that, masking of $I_{gchannel}$ is performed with the mask obtained. This step removes background noise and unwanted pixels that do not constitute ROI as shown in Fig. 4. Instead of a

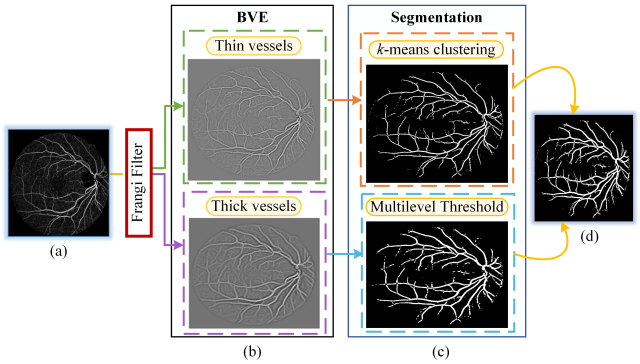

Fig. 5: Flow diagram showing blood vessels enhancement, segmentation and image fusion. (a) Pre-processed image. (b) BVE module: Application of Frangi filter generated two outputs (Thin vessels network and thick vessels network). (c) Segmentation module: k-means clustering used for thin vessels network and Multilevel Thresholding used for thick vessels network. (d) Image fusion: Final segmented image obtained by fusion of thick and thin vessels.

normal top-hat transform which induces noise, modified top-hat transform [36] is adopted. Modified top-hat ensures better noise removal and suitable feature extraction.

$$I_{Tophat} = I - (I \bullet S_c)\ o\ S_o \tag{1}$$

where I is input image, $\bullet$ is a closing operator, o is an opening operator, S_c is the structuring element used for closing and S_o is the structuring element for opening, I_{Tophat} is the output image. For both closing and opening disk type structuring element with the radius of 15 pixels is used. The opening stage of the modified top-hat transform removes the optic disc. Fig. 4(a) has the clear optic disc, macula, and noisy background. Proposed NVCR completely removes these NVC without effecting the blood vessels in the optic disc region as shown in Fig. 4(b).

3) Blood Vessels Enhancement (BVE): Without BVE, the output generated by NVCR will be directly subjected to the segmentation module. It is clearly evident from Fig. 4(b) that the output of NVCR is not appropriate for vasculature segmentation. It needs proper enhancement before segmentation. Hence, BVE is a crucial factor for blood vasculature enhancement and to make image appropriate for segmentation. Currently used enhancement techniques also enhance noise that appears as spurs in the segmented result and increases false positive rate. Frangi filter is used in this work for blood vessels enhancement. Contrary to existing techniques that enhance whole structure, Frangi filter performs enhancement of only elongated structures. In the case of retinal images, these structures constitute blood vessels. Thus, the noise is suppressed as shown in Fig. 5(b). Given a continuous 2D image $I(\hat{Y}\ )$, Frangi filter [37] for blood vessel enhancement is adopted.

$$r(\hat{Y},\sigma,\beta_1,\beta_2) = \begin{cases} 0 & \text{if } \lambda_2(\hat{Y},\sigma) > 0 \\ \exp\left(-\dfrac{R_B^2(\hat{Y},\sigma)}{2\beta_1^2}\right)\times & \\ \left(1-\exp\left(-\dfrac{S^2(\hat{Y},\sigma)}{2\beta_2^2}\right)\right), & \text{otherwise} \end{cases} \tag{2}$$

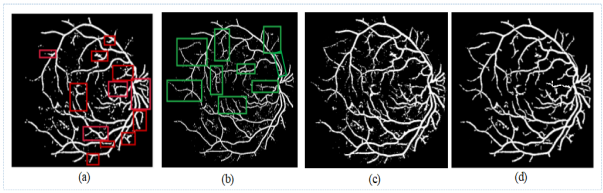

Fig. 6: (a) Vasculature estimated by multi-level Otsu threshold. The highlighted portion is estimated only by multi-level threshold. (b) Vasculature estimated by k-means. The highlighted portion is estimated only by k-means. (c) Image fusion: combines and harness results of both (a) and (b) to create a single-fused image (I_{fused}). I_{fused} is more informative, as it combines information from both (a) and (b). (d) Post-processing: Result obtained by performing area opening of I_{fused}.

where $\lambda_1(\hat{Y},\sigma)$ and $\lambda_2(\hat{Y},\sigma)$ are eigenvalues of local hessian estimated at $\hat{Y}$ with scale σ. $R_B(\hat{Y},\lambda) = \frac{\lambda_1(\hat{Y},\sigma)}{\lambda_2(\hat{Y},\sigma)}$ is the elongated strength. It calculates the variation from blob by taking into account the eccentricity of the second ellipse. The structureness measure is given by $S(\hat{Y},\sigma) = \sqrt{\lambda_1^2(\hat{Y},\sigma)+\lambda_2^2(\hat{Y},\sigma)}$. The parameters β_1 (Frangi beta one) and β_2 (Frangi beta two) control sensitivity of the filter to deviation in $R_\beta(\hat{Y},\sigma)$ and $S(\hat{Y},\sigma)$ [38]. The values used for β_1 and β_2 are 2 and 3.5.

B. Segmentation

Segmentation is paramount of overall performance because the errors prevailing in final segmented retinal images will significantly affect the feature extraction and identification process. In phase-based level set methods, vessel width plays an important role in the wavelet response. Thick blood vessels give a high response in contrast to thin vessels [15]. Due to varying wavelet response, thin vessels may get discarded. Another overhead of such methods is the optimal threshold selection to handle varying wavelet response. To overcome these issues and to retain both thick and thin vessels hybrid segmentation technique is used. Hybrid segmentation technique aids to estimate as much vasculature as possible. That in turn helps to achieve high segmentation accuracy. The advantage and contribution of hybrid segmentation are evident from Fig. 6. k-means clustering is used for thin vessels segmentation. k-means is a data clustering iterative algorithm that partitions the data points into clusters on the basis of their distances from the centroid [39]. To choose clusters k optimal for our data set, average silhouette method [40], [41] is used. Multi-level thresholding using Otsu is used for thick blood vessels segmentation. It performs well where the image has to be divided into two classes of pixels. It automatically calculates the optimum threshold in such a way that it maximizes between class variance of segmented classes [35]. It divides the image into multiple classes with optimization objective as:

$$J_1(th_1, th_2, ...th_k) = {\sigma_0}^2 + \sigma_1^2 + \sigma_2^2 + ... + \sigma_k^2 \tag{3}$$

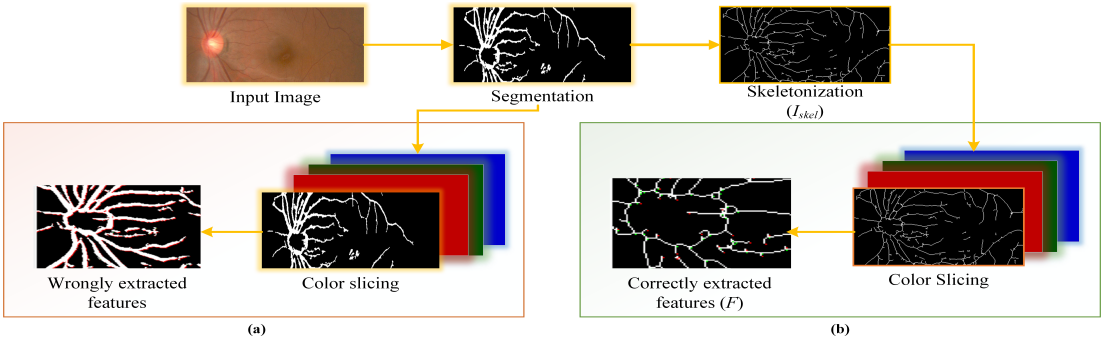

Fig. 7: Two possible outcomes of the feature extraction phase. (a) The result of feature extraction performed without skeletonization. Consequently, the feature extraction generates wrong features. (b) The result of feature extraction performed with skeletonization. The extracted features are correct and each one is marked correctly by color slicing.

where k is the total number of classes, $\{th_1, th_2, ..., th_k\}$ is the set of thresholds applied on the image, and $\{\sigma_0^2, \sigma_1^2, \sigma_2^2, ..., \sigma_k^2\}$ is variance set.

After segmentation, image fusion is performed to harness the results generated by k-means and multi-level threshold to generate a single-fused image. Image fusion is performed by spatial domain fusion method. We particularly used pixel level fusion using the Maximum method from spatial domain [42]. The maximum method performs a selection process. Every corresponding pixel of the images to be fused is compared. After that, the pixel with the maximum intensity is selected and placed on the corresponding position of the resultant image. Thus, every pixel of the fused image is the maximum intensity of the corresponding position pixels in the input images.

$$I_{fused}(i,j) = \sum_{i=1}^{M} \sum_{j=1}^{N} max(X_1(i,j), X_2(i,j), ..., X_n(i,j)) \quad (4)$$

where $X_1, X_2, ..., X_n$ are the input images, I_{fused} is the output fused image, n is the total number of images to be fused, $max()$ finds the maximum intensity pixel, M and N correspond to the total number of rows and columns. The reason for opting out this particular method is that it does not compromise over the good information available in the image, it is fast and efficient. Its disadvantage is that the maximum pixel is not always the better pixel. However, it is rectified in our method by post-processing. As evident from Fig. 6(c), I_{fused} is more informative as compared to results generated by the individual segmentation. As proposed segmentation retains both vessels, so it outperforms the other existing segmentation techniques and have high accuracy.

C. Post-Processing

Before analyzing I_{fused} for identification, it is subjected to post-processing to get rid of spurs and unwanted regions produced during segmentation. Area opening is used to remove these artifacts. In this paper, vessels that have less than or equal to 20 pixels are regarded as unwanted regions and are discarded out. The result of area opening is shown in Fig. 6(d). Before feature extraction, it is necessary to reduce vessels width to 1. Without width reduction, the feature extraction stage will yield incorrect features as evident from Fig. 7(a). Width is reduced by skeletonization. For skeletonization, MATLAB's built-in morphological function named $bwmorph$ is used [43]. $I_{skel} = bwmorph(bw,' skel', Inf)$ where bw is the segmented image obtained after area opening, with Inf $bwmorph$ repeats the operation until there is no further change in the image. Fig. 7 shows a step-wise illustration of feature extraction performed with and without skeletonization.

D. Feature Extraction

Like other biometric identification systems, retinal identification also relies on its unique features to distinguish subjects from one another. These include (a) end point (end of a vessel), (b) bifurcation (where a vessel splits into two), (c) crossing over (the point where two vessels meet up) as shown in Fig. 1. To ensure maximum discriminant power and high accuracy, we used all three of them. For feature extraction, crossing number technique is used. It takes the skeleton image I_{skel} as input and outputs an image with extracted features F (Fig. 7).

$$CN(P) = \frac{1}{2} \sum_{i=1}^{8} |I_{skel}(p_i) - I_{skel}(p_{i+1})| \quad (5)$$

where P is the pixel to be evaluated, p_i are the pixels surrounding P in a clockwise direction and I_{skel} is the skeleton image. CN is half of the sum of the difference between adjacent pixels in the 8-neighborhood of P. Algorithm 1 is the pseudocode for crossing number and color slicing. CN explores 8-neighbourhood of a pixel that constitutes vessel in a clockwise direction. Depending on final CN value, a pixel is designated either as a feature point or not. Color slicing is used to highlight the detected feature points. For color slicing, a matrix with 3 layers (Clr_img) having the same dimension as that of I_{skel} is initialized. Corresponding to CN value, a specific color (Red for end point, Green for bifurcation, Blue for crossing over) is stored at the same location in Clr_img. Once feature extraction is completed, Clr_img is superimposed on I_{skel}. Before superimposition, I_{skel} is also concatenated in 3 dimensions to have an image with three layers (N_Img). Superimposition of Clr_img on N_Img gives the final image F with all extracted features highlighted as shown in Fig. 7(b).

Algorithm 1 Feature Extraction and Color Slicing

Require: Skeleton Image I_{skel}
Ensure: Final Image with extracted features F
Do zero padding of I_{skel} to obtain a matrix img;
Initialize a matrix Clr_Img (with three layers) having the same size as that of I_{skel} for color slicing;
for $\forall\ p \in img$ **do**
  if $img[p] == 1$ **then**
    Calculate CN value using Eq. (5);
    Color Slicing: Evaluate computed CN value;
    if $CN == 1$ **then**
      $p\ \ is\ end\ \ point$;
      $Clr\_Img[p] \leftarrow Red\ Color$;
    else if $CN == 3$ **then**
      $p\ is\ bifurcation$;
      $Clr\_Img[p] \leftarrow Green\ Color$;
    else if $CN > 3$ **then**
      $p\ is\ crossing\ over$;
      $Clr\_Img[p] \leftarrow Blue\ Color$;
    end if
  else
    Move to $img_{(p+1)}$;
  end if
end for
N_Img = cat$(3, I_{skel}, I_{skel}, I_{skel})$;
F = N_Img + Clr_img;

E. Template Generation

1) Template Formulation: Once features are extracted, the next step is to formulate templates and store them in the database. The matching phase is paramount for the identification process. Irrespective of rotation and translation, the angle and distance between different feature points remain the same. This consistency is harnessed to ensure that matching is rotation and translation invariant. The angle and distance between a candidate feature point and its four nearest feature points are calculated to formulate a template. Resulting template is of dimension $R \times 8$. Where R is the number of features and varies for every image.

2) Dimensionality Reduction: The increase in template dimensionality makes pattern detection difficult. It slows down the matching process and makes it more complex. Feature extraction phase yields templates of varying dimensionality. Most of the existing retinal identification techniques focused only on accuracy and not on time efficiency. To make proposed matching process time efficient it is hastened by reducing template dimensionality. The proposed approach used PCA for dimensionality reduction. PCA is used because it converts the set of features into a reduced number of uncorrelated features. PCA ensures that principal components not only correspond to maximum variance, but also ensures that resulting set of features in the subspace are uncorrelated while retaining most of the information content [44], [45]. This guaranteed un-correlation improves the predictive performance of resulting features. The enhanced predictive power improves the performance of the classifier. The new retinal features are

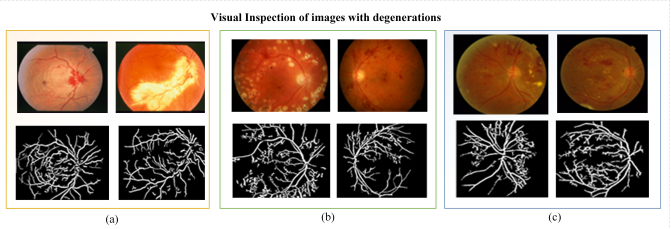

Fig. 8: Performance of proposed method on images with large degenerations. The first row corresponds to input images. The second row corresponds to the result of segmentation achieved by the proposed method. (a) Images from STARE [46] (b) Images from DIARETDB0 [47] (c) Images from Messidor [48].

termed as retinal Eigen features. Every original retinal feature is transformed into an Eigen value. Firstly, every image is converted into a column vector and stacked into a matrix i.e. $M = \{M_1, M_2, ..., M_N\}$. The zero-mean vector of each vector is found by subtracting the vector from mean:

$$x_0 = \frac{1}{N}\sum_{i=1}^{N} M_i - \bar{x} \rightarrow \bar{x} = \sum_{i=1}^{N} x_{i,j}/N \tag{6}$$

where x_0 is zero-mean vector, M_i is i^{th} column vector in matrix M, $x_{(i,j)}$ is $(i,j)^{th}$ entry in the vector M, $\bar{x}$ is mean and $i = 1, ..., N$. After mean, covariance matrix is computed as:

$$C = (x_0)(x_0)^T \tag{7}$$

where C is the covariance matrix, x_0 is zero mean vector, T is transpose and x_0^T is the transpose of zero mean vector. As C is large dimensionality matrix, Eigen vectors are calculated to obtain distinguishing features and remove redundant ones as:

$$C_v = \lambda E_v \tag{8}$$

where λ is Eigen value, E_v is Eigen vector and C_v is the matrix associated with Eigen values λ of vector E_v. All the images are transformed to Eigen subspace as:

$$y = W^T(M_i) \qquad i = \{1, 2, ..., N\} \tag{9}$$

where y is Eigen subspace termed as principal components or retinal Eigen features, W is projection matrix constructed from selected Eigen vectors, T is transpose and W^T is transpose of projection matrix. The first N Eigen features with high variance are selected. As a result, dimensionality is reduced. The resulting retinal Eigen features are stored in the database.

Without PCA, all templates will have varying dimension. With the increase in database and template size, identification will take more time and will be inappropriate for real-time applications. PCA significantly reduced the dimension of the templates. As a result, the time interval between matching and identification process is reduced. Consequently, the proposed technique takes less time in matching and is computationally more efficient. The statistical details of time efficiency achieved by the proposed technique are discussed later in Section VI-A.

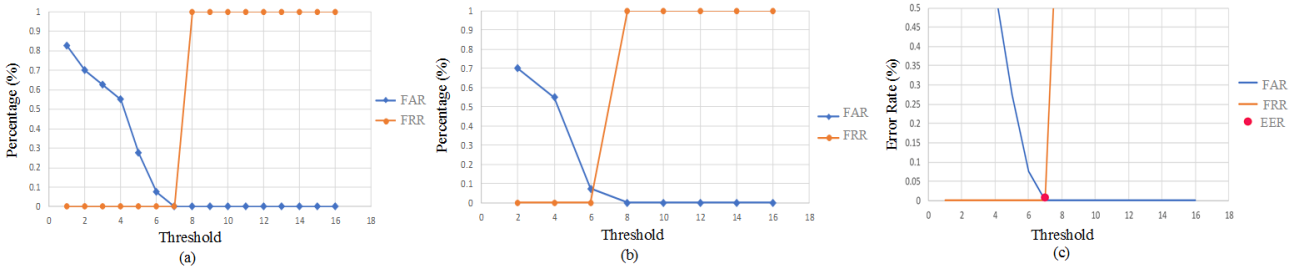

Fig. 9: FAR and FRR curves for retinal identification. (a) and (b) show the dependence of FAR and FRR on the threshold. (c) FAR and FRR with respect to the error rate. The intersection point represents EER, which is demonstrated by a magenta circle. As our approach has EER = '0', thus it is accurate.

V. Identification Module

When an unknown subject sample is given, the system generates its live-template. L2-norm given in Eq. (10) is used to calculate the feature distance between the feature vector of live-template and the feature vector of all the templates stored in the database.

$$||v|| = \sqrt{\sum_{i=1}^{k} |v_i^2|} \tag{10}$$

where v is a vector, k is the total number of elements in vector v and $|v_i^2|$ is absolute of squared values in v. To evaluate the similarity between samples, total similarity measure (TSM) is calculated. Whenever the live-template feature vector has minimum feature distance with some stored template feature vector, then the TSM for that subject is incremented by '1'. TSM is calculated as:

$$TSM = Subject\ ID[find(min_i(FD))] + 1, i = 1....N \tag{11}$$

where $find()$ is a MATLAB's built-in function that finds the index position, $min()$ is a MATLAB's built-in function that returns the minimum element, FD is the feature distance, $Subject\ ID$ is an array having the same length as that of the number of subjects stored in the database and is used for keeping the matching score, N is the total number of templates stored in the database. With $find(min(FD))$ index position where the minimum value of FD is encountered is found. After that, an increment of 1 is done to that index of the $Subject\ ID$. The result of this matching is a list of TSM values. After the live-template has been compared with all the templates in the database the final decision is made by comparing maximum TSM with a threshold as:

$$max(TSM) \geq T \tag{12}$$

where T is the threshold. If the above condition is satisfied, then the query image is regarded as authenticated. Otherwise, it is rejected as an intruder. Thresholding step is vital for rejection of intruders.

VI. Experimental Results

The algorithm is implemented and tested using MATLAB R2015b environment on a workstation with Intel(R) CORE(TM) i3-4130, 3.40GHz, and 8GB RAM. In contrast to face recognition, very few databases are available for retinal identification. To the best of our knowledge, VARIA [49] and RIDB [50] are the only publicly available databases for retinal identification purpose. For this reason, we created our own database named Biometric Retinal Identification Database (BRDB). Other existing techniques have evaluated performance on some local database or on publicly available databases like DRIVE [51] and STARE [46]. Local databases are not publicly available. Hence for a fair comparison with these techniques and to make publicly available databases suitable for identification, augmentation is used to generate multi-samples per subject. Each image is rotated randomly to generate nine samples per subject. For performance evaluation on pathological images STARE [46], HRF [52], Messidor [48], DIARETDB0 [47] are used. Experimental section is further divided into two subsections: Retinal Identification and Retinal Vasculature Segmentation.

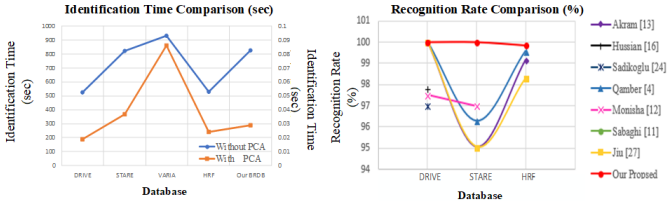

Fig. 10: (a) Identification time comparison performed with and without PCA. Our approach has significantly accelerated the matching. (b) Recognition rate comparison of different techniques. Our approach has the highest recognition rate.

A. Retinal Identification

Proposed approach authenticity is evaluated by conducting different experiments. A personal database BRDB is designed to evaluate the validity of the proposed technique. BRDB consists of 1800 color retinal images of 200 subjects with nine samples per subject. Images are captured using Fundus camera TOPCON TRC NW300, having 8M pixels per inch (PPI), and are non-mydriatic with a 45-degree field of view. The images are macular centered, have the dimension of (1536x2048x3) and are stored in .JPG format. To evaluate proposed technique performance, 60 subjects were selected to act as authenticated users. Out of 9 samples, 6 samples are used for training and 3 samples are used for testing. 70 subjects were selected to act as intruders. This set-up created a total of 810 experiments ($60 \times 3 = 180$ authenticated subjects experiment, $70 \times 9 = 630$

TABLE I: Performance comparison for retinal identification

No.	Method	Database	Total Images	Correctly Recognized	Wrongly Recognized	Accuracy %	Identification Rate%
1	Akram et al. [13]	DRIVE STARE VARIA	40 81 233	40 77 231	0 4 2	100 95.05 99.14	98.30
2	Hussain et al. [16]	DRIVE	40	39	1	97.50	97.50
3	Sadikoglu and Uzelaltinbulat [24]	DRIVE	-	-	1	97.50	97.50
4	Qamber et al. [4]	DRIVE STARE VARIA	40 81 233	40 78 232	0 3 1	100 96.29 99.57	98.87
5	Monisha and Seldevchristopher [12]	DRIVE STARE	40 100	39 97	1 3	97.5 97	98.87
6	Sabaghi et al. [11]	DRIVE	40	40	0	100	100
7	Jiu et al. [27]	DRIVE STARE VARIA	- - -	- - -	- - -	100 95.06 98.28	97.78
8	Fatima et al. [15]	VARIA RIDB	233 100	232 97	1 3	99.57 97	98.28
9	Farzin et al. [17]	DRIVE+STARE	300	-	-	99.0	99.0
10	Köse et al. [25]	STARE	80	-	-	95.0	95.0
11	**Our Proposed**	DRIVE STARE VARIA RIDB **Our BRDB**	40 81 233 100 1800	40 81 232 98 1797	0 0 1 2 3	100 100 99.57 98 99.46	99.40⋆

⋆ **Other techniques have only used DRIVE, STARE, VARIA or RIDB. Due to this in some cases, their average identification rate is more as compared to our proposed technique. In contrast, our method is evaluated on all of them including BRDB. The proposed method achieved the highest accuracy database wise.**

TABLE II: Performance evaluation on images with degenerations

Database	Total Images	Correctly Recognized	Wrongly Recognized	Identification Rate (%)
STARE [46]	400	399	1	99.75
HRF [52]	45	45	0	100
Messidor [48]	800	797	3	99.62
DIARETDB0 [47]	130	128	2	98.46

intruder experiments). The proposed approach achieves the highest recognition rate that makes it more effective. It outperforms other existing techniques as clearly evident from Table I. For pathological cases, effectiveness of technique is evaluated using STARE [46], HRF [52], Messidor [48] (first two sets) and DIARETDB0 [47]. The statistical results of performance with these databases are given in Table II. It is evident that the proposed technique achieves a high identification rate even with these databases. Fig. 8 shows the visual results obtained with these databases. The results clearly depict proposed technique strength to deal with images having degenerations. The proposed approach is further validated by False acceptance rate (FAR), False rejection rate (FRR) and Equal error rate (EER). These matrices vary according to the chosen threshold. There is always a trade-off between FAR and FRR. Fig. 9 shows the effect on FAR and FRR with respect to change in threshold values. The intersection point of FAR and FRR represents EER. From Fig. 9(c), it is clear that the proposed method achieves an EER of zero which makes it completely accurate and gives it a lead over existing techniques.

1) Identification Time: Biometric systems have to be used in real time, so they must be computationally accelerated and time efficient. Our method achieved this acceleration by using PCA. PCA reduced dimensionality and decreased the time interval between matching and identification process. The statistical details of time efficiency achieved by the proposed technique is given in Table III. The identification time for the techniques without any acceleration ranges from 500 - 900 seconds. On the other hand, the proposed technique significantly reduced it to a range of 0.019 - 0.029 seconds. Average time clearly shows that the proposed approach is much more efficient. This efficiency makes the proposed method more appropriate for real-time applications. Fig. 10(a) shows acceleration achieved by the proposed method as compared to techniques without any acceleration mechanism. Thus experimental results showed that our method has low computational time and outperforms techniques without any acceleration mechanism. The total identification time comprises of a fixed time (required for retinal image pre-processing, segmentation and feature extraction) and a variable time for the one-to-many matching process. Total identification time is calculated as:

$$Total\_identification\_time = Fixed\ Time + TL(one - to - one\ template\ matching) \quad (13)$$

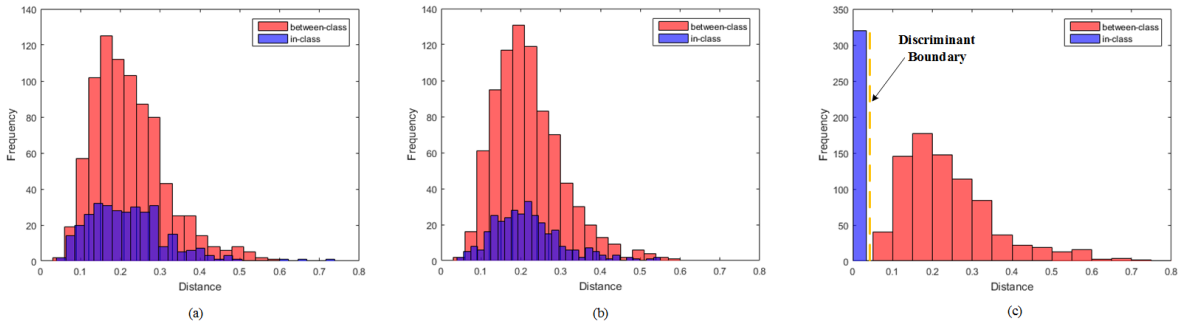

Fig. 11: Discriminant power comparison. (a) End points as feature points. (b) Bifurcation as feature points. Clearly, in both (a) and (b), there is overlapping of in-class and between-classes distances. Thus, subjects are not identified correctly. (c) The proposed combination of features points. There is no overlapping and there is a clear discriminant boundary among classes.

TABLE III: Identification time comparison with/without PCA

Database	Total Images	Query Image Name	Total Identification Time (sec)	
			Without PCA	With PCA
DRIVE [51]	40	38_training.tif	523.19	0.019
STARE [46]	100	Im0038.ppm	821.77	0.037
VARIA [49]	233	012.pgm	930.28	0.086
HRF [52]	45	08_h.jpg	529.27	0.024
Our BRDB	1800	4.jpg	827.20	0.029
Average Time	-	-	736.342	**0.039**

TABLE IV: Comparison for retinal vasculature segmentation

Method	DRIVE			STARE		
	Acc	Sn	Sp	Acc	Sn	Sp
Staal et al. [51]	0.944	0.719	0.977	0.952	0.697	0.981
You et al. [53]	0.943	0.741	0.975	0.950	0.726	0.976
Soares et al. [54]	0.946	0.724	0.976	0.948	0.710	0.974
Singh and Srivastava [55]	0.952	0.759	0.971	0.927	0.794	0.938
Imani et al. [56]	0.952	0.752	0.975	0.959	0.750	0.975
Vlachos and Dermatas [57]	0.929	0.747	0.955	-	-	-
BahadarKhan et al. [58]	0.961	0.746	0.980	0.946	0.758	0.963
Our Proposed	0.968	0.756	0.978	0.963	0.755	0.963

where TL is the total number of templates stored during registration, $Fixed\ Time$ is 0.316 seconds, and $one-to-one\ template\ matching$ time is 0.0079 seconds (on a workstation with Intel(R) CORE(TM) i3-4130, 3.40GHz and 8GB RAM).

2) Feature Comparison: Selected features discriminant power is evaluated by comparing it with different kinds of features (end points, bifurcations and proposed combination of end points, bifurcations and crossing over). Performance of all these features is evaluated and compared by the following experiment. FD between the live-template of different subjects and registered subjects is calculated. If the template belongs to the same class, then distance is categorized as in-class. Otherwise, the distance is categorized as between-class. The distribution of the two distances is approximated as histograms. Intuitively, if a feature has good discrimination power, then there will be no overlapping between both kinds of distances and there will be a clear distinction among classes. The histograms obtained as a result of this experiment are shown in Fig. 11. When end points and bifurcations are used independently, there is an overlapping of between-class and in-class distance. However, with the proposed combination there is no overlap and there is a clear discriminant boundary among classes. Hence, the identification phase leads to correct results with high accuracy.

3) The Impact of Scaling on System Performance: The impact of scaling has been analyzed in terms of execution time, identification rate and an average number of extracted features as shown in Fig. 12. For analyzing the impact of scaling on system performance, we downsampled the images from the original resolution. The images are resampled to the resolutions of 512×512, 256×256, 128×128, 64×64, 32×32 and 16×16 respectively. Fig. 12(c) shows that

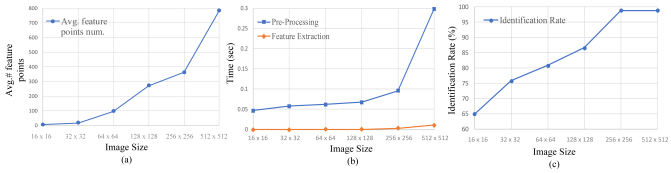

Fig. 12: (a) Scaling effect on average feature points number. (b) Scaling effect on time consumed in pre-processing and features extraction. (c) Scaling effect on identification accuracy.

the identification rate with the resolution of 512×512 and 256×256 is the same i.e. 99.85%. However, the execution time with the resolution of 256×256 is faster as compared to the resolution of 512×512. With the resolution of 16×16 execution time is fastest, but the identification rate declines to 65%. So for the optimal performance, all the images are downsampled to the resolution of 256×256. With the increase in image size, the number of extracted feature increases correspondingly. However, with the increased number of extracted features execution time increases which make the identification process slow.

B. Retinal Vasculature Segmentation

To evaluate proposed technique performance for segmentation it has been validated on DRIVE [51], STARE [46] and has been compared with other existing techniques. The performance is evaluated with respect to three evaluation measures i.e. Accuracy (Acc), Sensitivity (Sn) and Specificity (Sp). The statistical results of this comparison are given in Table IV. The proposed segmentation is very efficient

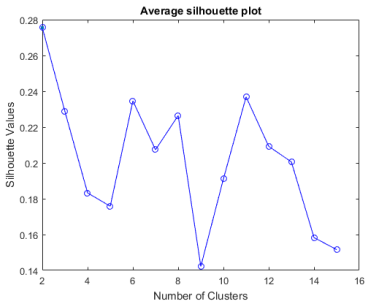

Fig. 13: Average silhouette plot for computing k. The plot peak value is 2. So $k = 2$ is proper cluster choice.

and achieved the highest accuracy as compared to all other paralleled techniques. Our method also achieved highest Sn and Sp for DRIVE except for Singh [55] and Bahadar Khan [58] which is only better comparatively by a difference of 0.003 and 0.002. While in the case of STARE, Sn of Singh [55] and Bahadar Khan [58] are 0.039 and 0.003 better. The Sp of You [53], Soares [54] and Imani are slightly better by 0.013, 0.011 and 0.012 respectively. Fig. 8 shows the effectiveness of our segmentation technique. The experimental results validate that the suggested method is very effective as compared to other cited frameworks. To choose number of clusters (k) of k-means clustering that are optimal for segmentation of our data set, average silhouette method [40], [41] is used. We computed k-means clustering by varying k from 1-15. For each k, the average silhouette of observations is then calculated. The maximum location of average silhouette plot is considered as the appropriate number of clusters [40], [41]. As evident from Fig. 13, the maximum location of average silhouette plot for our data set is observed at 2. So, the value of k is set to 2.

VII. Conclusion

A fast and accurate automated retinal identification system is developed. Experimental results showed an identification rate of 99.40% with the EER of zero. In contrast to other techniques, it achieves high identification accuracy by using such set of features that offer maximum discriminant power and completely eliminated overlap among classes. Our approach has low computational time and is computationally more efficient. Proposed segmentation technique is found to be more efficient and improved segmentation accuracy to 99.65%. The limitation of this work is that with images having severe pathological noise the identification rate is low as compared to normal images. The reason for this decline is that in presence of severe pathological disorder it is difficult to extract the feature points. Due to this difficulty, another limitation arises, i.e. identification time for such images is more as compared to normal ones. In the future, we will overcome this limitation by particularly improving our image enhancement module. Improved image enhancement will yield more enhanced images for pathological cases as well. That, in turn, will aid the feature extraction phase. This convenient feature extraction will overcome will make the identification process fast for pathological cases as well. Alongside we plan to create an even more larger retinal database, with images taken over even much longer periods and improve performance by applying various discriminant analytics.

References

[1] M. Wazid, A. K. Das, N. Kumar, and J. J. P. C. Rodrigues, "Secure three-factor user authentication scheme for renewable-energy-based smart grid environment," *IEEE Trans. Ind. Informat.*, vol. 13, no. 6, pp. 3144–3153, 2017.

[2] F. Zhao, H. Luo, X. Zhao, Z. Pang, and H. Park, "HYFI: Hybrid floor identification based on wireless fingerprinting and barometric pressure," *IEEE Trans. Ind. Informat.*, vol. 13, no. 1, pp. 330–341, 2017.

[3] P. Hu, H. Ning, T. Qiu, Y. Zhang, and X. Luo, "Fog computing based face identification and resolution scheme in internet of things," *IEEE Trans. Ind. Informat.*, vol. 13, no. 4, pp. 1910–1920, 2017.

[4] S. Qamber, Z. Waheed, and M. U. Akram, "Personal identification system based on vascular pattern of human retina," in *Cairo International Biomedical Engineering Conference*, 2012, pp. 64–67.

[5] Z. Chen, Q. Zhu, Y. C. Soh, and L. Zhang, "Robust human activity recognition using smartphone sensors via CT-PCA and online SVM," *IEEE Trans. Ind. Informat.*, vol. 13, no. 6, pp. 3070–3080, 2017.

[6] K. Zinchenko, C.-Y. Wu, and K.-T. Song, "A study on speech recognition control for a surgical robot," *IEEE Trans. Ind. Informat.*, vol. 13, no. 2, pp. 607–615, 2017.

[7] A. K. Jain, A. Ross, and S. Pankanti, "Biometrics: A tool for information security," *IEEE Trans. Inf. Forensics Security*, vol. 1, no. 2, pp. 125–143, 2006.

[8] Z. Chen, L. Zhang, Z. Cao, and J. Guo, "Distilling the knowledge from handcrafted features for human activity recognition," *IEEE Trans. Ind. Informat.*, pp. 1–9, 2018.

[9] V. S. Joshi, M. K. Garvin, J. M. Reinhardt, and M. D. Abramoff, "Identification and reconnection of interrupted vessels in retinal vessel segmentation," in *IEEE International Symposium on Biomedical Imaging: From Nano to Macro*, 2011, pp. 1416–1420.

[10] Z. Waheed, M. U. Akram, A. Waheed, and A. Shaukat, "Robust extraction of blood vessels for retinal recognition," in *International Conference on Information Security and Cyber Forensics*, 2015, pp. 1–4.

[11] M. Sabaghi, S. R. Hadianamrei, A. Zahedi, and M. N. Lahiji, "A new partitioning method in frequency analysis of the retinal images for human identification," *Journal of Signal and Information Processing*, vol. 2, no. 4, pp. 274–278, 2011.

[12] L. S. Monisha and C. Seldevchristopher, "Biometric identification using retina scan," *International Journal of Advanced Research Trends in Engineering and Technology*, vol. 2, pp. 145–151, 2015.

[13] M. U. Akram, A. Tariq, and S. A. Khan, "Retinal recognition: Personal identification using blood vessels," in *International Conference for Internet Technology and Secured Transactions*, 2011, pp. 180–184.

[14] G. Sasidharan, "Retina based personal identification system using skeletonization and similarity transformation," *International Journal of Computer Trends and Technology*, vol. 17, no. 3, pp. 144–147, 2014.

[15] J. Fatima, A. M. Syed, and M. U. Akram, "A secure personal identification system based on human retina," in *IEEE Symposium on Industrial Electronics Applications*, 2013, pp. 90–95.

[16] A. Hussain, A. Bhuiyan, A. Mian, and K. Ramamohanarao, "Biometric security application for person authentication using retinal vessel feature," in *International Conference on Digital Image Computing: Techniques and Applications*, 2013, pp. 1–8.

[17] H. Farzin, H. Abrishami-Moghaddam, and M.-S. Moin, "A novel retinal identification system," *EURASIP Journal on Advances in Signal Processing*, vol. 2008, pp. 280 635:1–280 635:10, 2008.

[18] D. Kumar, A. Pramanik, S. S. Kar, and S. P. Maity, "Retinal blood vessel segmentation using matched filter and Laplacian of Gaussian," in *International Conference on Signal Processing and Communications*, 2016, pp. 1–5.

[19] M. M. Fraz, S. A. Barman, P. Remagnino, A. Hoppe, A. Basit, B. Uyyanonvara, A. R. Rudnicka, and C. G. Owen, "An approach to localize the retinal blood vessels using bit planes and centerline detection," *Computer Methods and Programs in Biomedicine*, vol. 108, no. 2, pp. 600–616, 2012.

[20] G. Azzopardi, N. Strisciuglio, M. Vento, and N. Petkov, "Trainable COSFIRE filters for vessel delineation with application to retinal images," *Medical Image Analysis*, vol. 19, no. 1, pp. 46–57, 2015.

[21] M. U. Akram, I. Jamal, A. Tariq, and J. Imtiaz, "Automated segmentation of blood vessels for detection of proliferative diabetic retinopathy," in *IEEE-EMBS International Conference on Biomedical and Health Informatics*, 2012, pp. 232–235.

[22] J. Zhu, Z. Ge, and Z. Song, "Distributed parallel PCA for modeling and monitoring of large-scale plant-wide processes with big data," *IEEE Trans. Ind. Informat.*, vol. 13, no. 4, pp. 1877–1885, 2017.

[23] M. Womack, "The eyes have it," *Sensor Review*, vol. 14, no. 4, pp. 15–16, 1994.

[24] F. Sadikoglu and S. Uzelaltinbulat, "Biometric retina identification based on neural network," *Procedia Computer Science*, vol. 102, pp. 26–33, 2016.

[25] C. Köse, C. İki *et al.*, "A personal identification system using retinal vasculature in retinal fundus images," *Expert Systems with Applications*, vol. 38, no. 11, pp. 13 670–13 681, 2011.

[26] M. A. El-Sayed, M. Hassaballah, and M. A. Abdel-Latif, "Identity verification of individuals based on retinal features using Gabor filters and SVM," *Journal of Signal and Information Processing*, vol. 7, pp. 49–59, 2016.

[27] F. Jiu, K. Noronha, and D. Jayaswal, "Biometric identification through detection of retinal vasculature," in *IEEE International Conference on Power Electronics, Intelligent Control and Energy Systems*, 2016, pp. 1–5.

[28] J. Wei and G. Li, "Automated lung segmentation and image quality assessment for clinical 3-D/4-D-computed tomography," *IEEE J. Transl. Eng. in Health and Med.*, vol. 2, pp. 1–10, 2014.

[29] M. S. Haleem, L. Han, J. van Hemert, B. Li, and A. Fleming, "Retinal area detector from scanning laser ophthalmoscope (SLO) images for diagnosing retinal diseases," *IEEE J. Biomed. Health Informat.*, vol. 19, no. 4, pp. 1472–1482, 2015.

[30] A. Tariq and M. U. Akram, "An automated system for colored retinal image background and noise segmentation," in *IEEE Symposium on Industrial Electronics and Applications*, 2010, pp. 423–427.

[31] N. P. Ward, S. Tomliivson, and C. J. Taylor, "Image analysis of fundus photographs: The detection and measurement of exudates associated with diabetic retinopathy," *Ophthalmology*, vol. 96, no. 1, pp. 80–86, 1989.

[32] A. F. M. Hani, T. A. Soomro, I. Fayee, N. Kamel, and N. Yahya, "Identification of noise in the fundus images," in *IEEE International Conference on Control System, Computing and Engineering*, 2013, pp. 191–196.

[33] K. Zuiderveld, *Graphics Gems IV*. San Diego, CA, USA: Academic Press Professional, Inc., 1994, ch. Contrast Limited Adaptive Histogram Equalization, pp. 474–485.

[34] S. Irshad, X. Yin, L. Q. Li, and U. Salman, "Automatic optic disk segmentation in presence of disk blurring," in *International Symposium on Visual Computing*, 2016, pp. 13–23.

[35] N. Otsu, "A threshold selection method from gray-level histograms," *IEEE Trans. Syst., Man, Cybern.*, vol. 9, no. 1, pp. 62–66, 1979.

[36] K. B. Khan, A. A. Khaliq, and M. Shahid, "B-COSFIRE filter and VLM based retinal blood vessels segmentation and denoising," in *International Conference on Computing, Electronic and Electrical Engineering*, 2016, pp. 132–137.

[37] A. F. Frangi, W. J. Niessen, K. L. Vincken, and M. A. Viergever, "Multiscale vessel enhancement filtering," in *International Conference on Medical Image Computing and Computer-Assisted Intervention*, 1998, pp. 130–137.

[38] S. Bouattour and D. Paulus, "Vessel enhancement in 2D angiographic images," in *International Conference on Functional Imaging and Modeling of the Heart*, 2007, pp. 41–49.

[39] C. K. Reddy and B. Vinzamuri, "A survey of partitional and hierarchical clustering algorithms," in *Data Clustering: Algorithms and Applications*, 2013.

[40] L. Kaufman and P. J. Rousseeuw, *Finding Groups in Data: An Introduction to Cluster Analysis*. Hoboken, NJ, USA: John Wiley & Sons, Inc., 2009.

[41] P. J. Rousseeuw, "Silhouettes: A graphical aid to the interpretation and validation of cluster analysis," *Journal of Computational and Applied Mathematics*, vol. 20, pp. 53–65, 1987.

[42] Y. B. Salem, K. Hamrouni, and B. Solaiman, "Image fusion models and techniques at pixel level," in *Image Processing, Applications and Systems (IPAS), 2016 International*. IEEE, 2016, pp. 1–5.

[43] R. C. Gonzalez, R. E. Woods, and S. L. Eddins, *Digital Image Processing Using MATLAB®*. Knoxville, TN, USA: Gatesmark Publishing, 2009.

[44] A. Gastounioti, S. Makrodimitris, S. Golemati, N. P. E. Kadoglou, C. D. Liapis, and K. S. Nikita, "A novel computerized tool to stratify risk in carotid atherosclerosis using kinematic features of the arterial wall," *IEEE J. Biomed. Health Informat.*, vol. 19, no. 3, pp. 1137–1145, 2015.

[45] R. F. Mansour, E. M. Abdelrahim, and A. S. Al-Johani, "Identification of diabetic retinal exudates in digital color images using support vector machine," *Journal of Intelligent Learning Systems and Applications*, vol. 5, pp. 135–142, 2013.

[46] A. Hoover and M. Goldbaum, "Locating the optic nerve in a retinal image using the fuzzy convergence of the blood vessels," *IEEE Trans. Med. Imag.*, vol. 22, no. 8, pp. 951–958, 2003.

[47] T. Kauppi, V. Kalesnykiene, J.-K. Kamarainen, L. Lensu, I. Sorri, H. Uusitalo, H. Kälviäinen, and J. Pietilä, "DIARETDB0: Evaluation database and methodology for diabetic retinopathy algorithms," Machine Vision and Pattern Recognition Research Group, Lappeenranta University of Technology, Finland, Tech. Rep., 2006.

[48] E. Decencière, X. Zhang, G. Cazuguel, B. Lay, B. Cochener, C. Trone, P. Gain, R. Ordonez, P. Massin, A. Erginay, B. Charton, and J.-C. Klein, "Feedback on a publicly distributed image database: the messidor database," *Image Analysis & Stereology*, vol. 33, no. 3, pp. 231–234, 2014.

[49] M. Ortega, M. G. Penedo, J. Rouco, N. Barreira, and M. J. Carreira, "Retinal verification using a feature points-based biometric pattern," *EURASIP Journal on Advances in Signal Processing*, vol. 2009, no. 1, pp. 235 746:1–235 746:13, 2009.

[50] Z. Waheed, M. U. Akram, A. Waheed, M. A. Khan, A. Shaukat, and M. Ishaq, "Person identification using vascular and non-vascular retinal features," *Computers & Electrical Engineering*, vol. 53, pp. 359–371, 2016.

[51] J. Staal, M. D. Abràmoff, M. Niemeijer, M. A. Viergever, and B. van Ginneken, "Ridge-based vessel segmentation in color images of the retina," *IEEE Trans. Med. Imag.*, vol. 23, no. 4, pp. 501–509, 2004.

[52] J. Odstrcilik, R. Kolar, A. Budai, J. Hornegger, J. Jan, J. Gazarek, T. Kubena, P. Cernosek, O. Svoboda, and E. Angelopoulou, "Retinal vessel segmentation by improved matched filtering: Evaluation on a new high-resolution fundus image database," *IET Image Processing*, vol. 7, no. 4, pp. 373–383, 2013.

[53] X. You, Q. Peng, Y. Yuan, Y. ming Cheung, and J. Lei, "Segmentation of retinal blood vessels using the radial projection and semi-supervised approach," *Pattern Recognition*, vol. 44, no. 10, pp. 2314–2324, 2011.

[54] J. V. B. Soares, J. J. G. Leandro, R. M. Cesar Jr., H. F. Jelinek, and M. J. Cree, "Retinal vessel segmentation using the 2-D Gabor wavelet and supervised classification," *IEEE Trans. Med. Imag.*, vol. 25, no. 9, pp. 1214–1222, 2006.

[55] N. P. Singh and R. Srivastava, "Retinal blood vessels segmentation by using gumbel probability distribution function based matched filter," *Computer Methods and Programs in Biomedicine*, vol. 129, pp. 40–50, 2016.

[56] E. Imani, M. Javidi, and H.-R. Pourreza, "Improvement of retinal blood vessel detection using morphological component analysis," *Computer Methods and Programs in Biomedicine*, vol. 118, no. 3, pp. 263–279, 2015.

[57] M. Vlachos and E. Dermatas, "Multi-scale retinal vessel segmentation using line tracking," *Computerized Medical Imaging and Graphics*, vol. 34, no. 3, pp. 213–227, 2010.

[58] K. BahadarKhan, A. A. Khaliq, and M. Shahid, "A morphological hessian based approach for retinal blood vessels segmentation and denoising using region based Otsu thresholding," *PLOS ONE*, vol. 11, no. 7, pp. e0 158 996:1–e0 158 996:19, 2016.